Section 2
ADVANCED TECHNOLOGY DEVELOPMENTS

2.A   Microstructural Control of Thin-Film Thermal Conductivity

Modeling of thin-film systems with absorbing inclusions[1] has indicated that thermal conductivity may play a role in laser damage of such films. Several studies have shown conclusively that thermal conductivity values for thin films are often lowered,[2-3] sometimes by an order of magnitude, from the thermal conductivity of corresponding bulk materials.

While mechanisms of thermal resistance have been well-characterized for bulk materials both theoretically and experimentally,[4] it is unclear which defects play primary roles in thin-film systems. Thermal-resistance mechanisms can be roughly divided into two categories; those for which the material may be treated as a continuum (voids, second phases), and those for which we must consider atomic-scale interactions in order to accurately predict thermal properties.

In this article, we seek to identify which thermal-resistance mechanisms are responsible for lowering thin-film thermal conductivity. To do this, measurements of the thin-film thermal conductivities for four systems are made, and the results interpreted in terms of the observed thin-film microstructures. Depending upon the film system studied, we use continuum and/or atomic-scale theoretical models to help illustrate which thermal-resistance mechanisms are at work.

While continuum thermal-conductivity-reduction mechanisms are easily understood and often straightforwardly modeled, by a rule of mixtures or a series of resistors, for example,[5] atomic-scale interactions require a more complicated

theoretical treatment. To simplify, we can assume that the primary heat carriers in a solid at room temperature are lattice vibrations (phonons), and charge carriers such as electrons. For a metal, both are important, while for a dielectric, like most of the materials used in thin-film optics, the primary contribution to heat conduction is from phonons. It is often convenient to treat phonons as particles encountering various scattering events as they propagate through a solid, leading to momentum loss or thermal resistance. We can express thermal conductivity K quite simply as

$$K = \frac{1}{3} Cvl ,$$ (1)

where C is the specific heat, v the velocity, and l the mean free path of the phonons. Equation (1) suggests clearly the effect of reducing the mean free path of phonons, or other heat carriers, on thermal-conductivity depression.

Expressions equivalent to Eq. (1) have been derived for thermal conductivity based on relaxation time,[6] or time between heat carrier-scattering events $\tau(x)$:

$$K = \frac{k_B}{2\pi^2 v} \left(\frac{k_B T}{\hbar} \right)^3 \int_0^{\Theta_D/T} \tau(x) \frac{x^4 e^x}{\left(e^x - 1 \right)^2} dx ,$$ (2)

where k_B = Boltzmann's constant, $\hbar$ = Planck's constant/2π, T is the absolute temperature, Θ_D is the Debye temperature, and v is the phonon or acoustic wave velocity. The term x is defined

$$x = \frac{\hbar \omega}{k_B T} ,$$ (3)

where ω is the phonon frequency. In turn, relationships have been developed that predict the effects of various defects on the relaxation time $\tau(x)$ and hence the thermal conductivity.[7-8] These theoretical relationships have been experimentally confirmed for many cases, including grain boundary and point-defect scattering.[9-10] In any event, evidence shows that a very small fraction of impurities or other defects can substantially lower thermal conductivity, both theoretically and experimentally.

We review data and microstructures for four thin-film systems; rare earth-transition metals (RE-TM), ZrO_2, $YBa_2Cu_3O_{7-\delta}$, and AlN. Each film is important in a specific application requiring dissipation of heat or knowledge of thermal transport: RE-TM for magneto-optical recording, ZrO_2 for optical-interference coatings, $YBa_2Cu_3O_{7-\delta}$ for superconducting microelectronics, and AlN for microelectronics and optics.

Experimental Techniques

Thermal conductivity of thin films is a difficult quantity to measure, and many techniques have been attempted. Here, we use the thermal-comparator technique, described in detail by Lambropoulos[2] et al. The thermal conductivity of a film/substrate system is measured by detecting the temperature drop of a metal probe brought into contact with the front face of the film, and comparing it to temperature drops recorded when the probe is in contact with materials of known

thermal conductivity. The substrate effect is removed via a solution of the heat-conduction equation for a thin film on a semi-infinite substrate, leaving a quantity K_{eff}, the thermal conductivity of the film including the effect of the film/substrate interfacial thermal resistance. The interfacial thermal resistance R_{int} can also be eliminated by measuring several thicknesses and treating the system as resistors in series, so that

$$\frac{t}{K_{eff}} = \frac{t}{K_f} + R_{int} ,$$ (4)

where t is the film thickness and K_f is the quantity of interest, the thermal conductivity of the film itself. Furthermore. by plotting t/K_{eff} versus t, as in Fig. 49.15, we obtain K_f from the inverse of the slope. The thermal conductivity of a thin film measured in this way is actually the thermal conductivity perpendicular to the plane of the film, since the dimension of the probe is much larger than that of the film thickness.
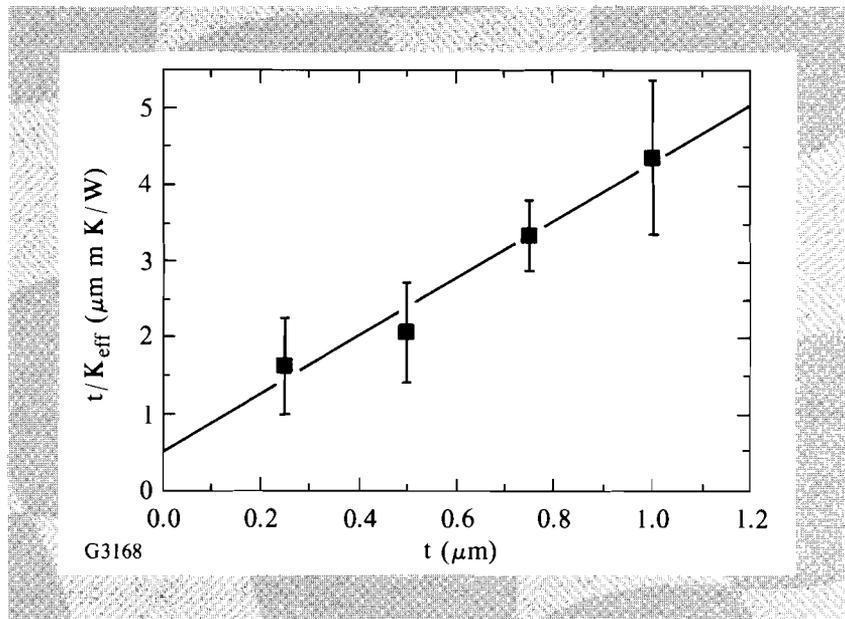

Fig. 49.15
Plot of Eq. (4) for a well-behaved system
($YBa_2Cu_3O_{7-\delta}$). 1/slope = film thermal conductivity K_f.

In the cases of the RE-TM and the $YBa_2Cu_3O_{7-\delta}$ films, it is also possible to measure the thermal conductivity in the plane of the film by using the Wiedemann-Franz-Lorenz conversion. Following the technique of Anderson,[11] the electrical sheet conductivity is measured directly by the four-point probe method, and converted via the Lorenz ratio to the electronic contribution to the thermal conductivity. The remaining contribution to the thermal conductivity, caused by phonon transport, is then estimated based on previous work and added to the electronic contribution to obtain a measure of K_f, this time in the plane of the film.

In order to determine the primary thermal-resistance mechanisms at work in each film system, the films were carefully characterized by a variety of techniques, including scanning electron microscopy (SEM), transmission electron microscopy (TEM), x-ray diffraction (XRD), infrared transmission spectroscopy (IR), x-ray photoelectron spectroscopy (XPS), and Rutherford backscattering (RBS).

The preparation conditions for each film material varied, and are mentioned in the discussion of each system.

RE-TM Films—Effect of Columnar Structure

A series of amorphous rare earth-transition metal (TbFeCoZr) films was sputtered from a single homogeneous target onto fused quartz substrates. In order to duplicate the variations in columnar morphology typically observed for metal films sputtered at various pressures,[12] the films were sputtered at three different pressures; 2 mTorr, 7 mTorr, and 15 mTorr.

Thermal conductivity was measured through the plane of the films $(K_\perp)$ using the comparator technique, and in the plane of the films $(K_\parallel)$ using the Wiedemann-Franz conversion technique described previously.[13] The values for $K_\perp$ and $K_\parallel$ are shown in Table 49.I for the three pressures. Noticeable trends are that $K_\parallel$ is generally smaller than $K_\perp$, and that it is significantly lower for the film deposited at the highest pressure.

Table 49.I: Thermal conductivity of RE-TM films.

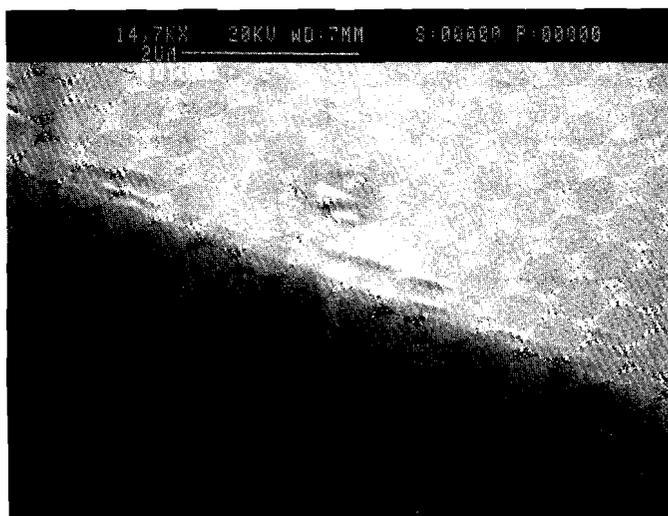| Deposition Pressure (mTorr)	$K_\perp$ (W/mK)	$K_\parallel$ (W/mK)
2	7.0	5.0
7	7.3	4.4
15	4.3	0.3

G3224

While the thermal conductivity of such a material in bulk form has never been reported, the thermal conductivity of a similar metallic glass FeNiCr has been calculated based on an estimate of the carrier mean free path as the interatomic distance. This projected value for bulk amorphous FeNiCr is 10 W/mK. The values for $K_\perp$ reported here are not much less than this, while the values for $K_\parallel$ are slightly reduced for the cases of 2- and 7-mTorr, and significantly reduced for the case of 15-mTorr deposition.

An explanation for the observed behavior is shown in the SEM micrographs of the film cross sections in Figs. 49.16–49.18. Note that as expected, the films become more columnar as deposition pressure is increased. Since the columns are oriented perpendicular to the film surfaces, heat can flow directly down the columns for the measurement of $K_\perp$, but must encounter internal intercolumnar contacts during the measurement of $K_\parallel$. The films are amorphous and the mean free paths of the heat carriers are on the order of the interatomic spacing, which is much less than the intercolumnar distance. Therefore, the concept of phonon or electron scatter is not particularly useful in describing the intercolumnar thermal resistance. Instead, we can treat the films as a continuum containing sources of internal resistance arranged in series in the film planes. From such a treatment, we can estimate the intercolumnar thermal contact resistance

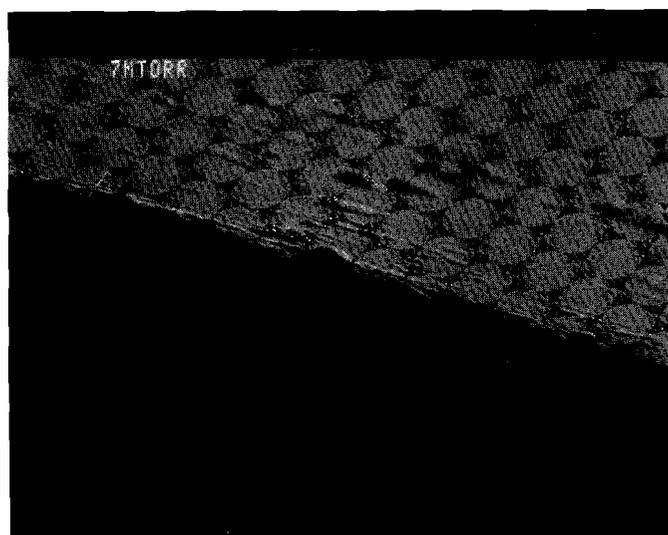$$\frac{w}{K_\parallel} = \frac{w}{K_\perp} + R_{\text{col}} , \tag{5}$$

where w is the column diameter, from Fig. 49.18 about 0.15 μm, and R_{col} is the intercolumnar contact resistance, which calculated from Eq. (5) is 4.7×10^{-7} m^{2}K/W. This is a very low thermal resistance compared with typical values for metal surfaces in contact,[14] indicating that there is little trapped gas (indicative of porosity) or other impurity content between the columns, which was confirmed by RBS. So, even very clean, dense films can have their thermal conductivities severely compromised, especially in the plane of the films, through the introduction of a columnar microstructure.

While we have investigated sputtered metal films, the same anisotropy should be observed for other sputtered films including dielectrics, as well as for evaporated and chemical-vapor-deposited films, which both typically show evidence of columnar or dendritic growth features.[15-16]
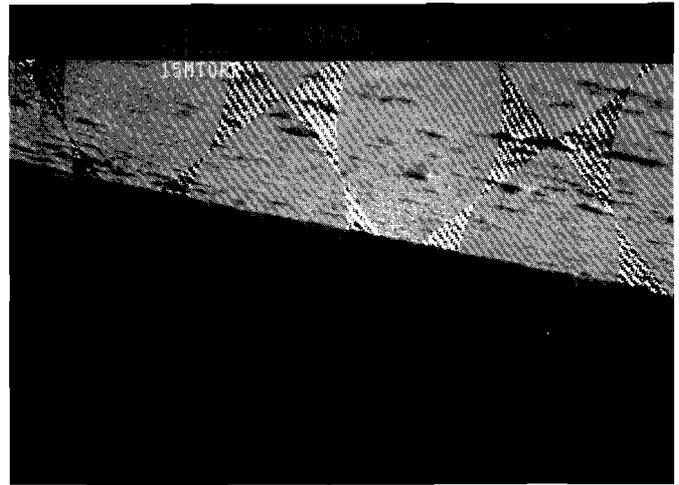

Fig. 49.16
SEM of TbFeCoZr cross section deposited at
2 mTorr.

G3169

Fig. 49.17
SEM of TbFeCoZr cross section deposited at
7 mTorr.

G3170

Fig. 49.18
SEM of TbFeCoZr cross section deposited at
15 mTorr.

G3171

ZrO$_2$—The Effect Of Variation in Crystal Structure

ZrO$_2$ films were e-beam evaporated from ceramic targets onto polished silicon, single-crystal (111)-oriented substrates. During deposition, the substrates were heated to 300°C.

The thermal-comparator method was used to obtain the thin-film thermal conductivity perpendicular to the plane of the films. The derivation of K_{eff}, the thermal conductivity of the film and film/substrate interface, yielded very unusual results. Figure 49.19 shows the plot of Eq. (4), which is generally used to extract the thermal conductivity of the film material. Comparison with the well-behaved plot in Fig. 49.15 shows the anomalous behavior inherent in the ZrO$_2$ films. Since all four thicknesses studied were deposited identically onto similar substrates, it is unlikely that the film/substrate interfacial resistance is varying. Therefore we conclude that the thermal conductivity of the thinner films is far too low compared with that of the thicker films. This renders it impossible to fit a positive slope to the data, making it impossible to extract a single reasonable value for the thin-film thermal conductivity.
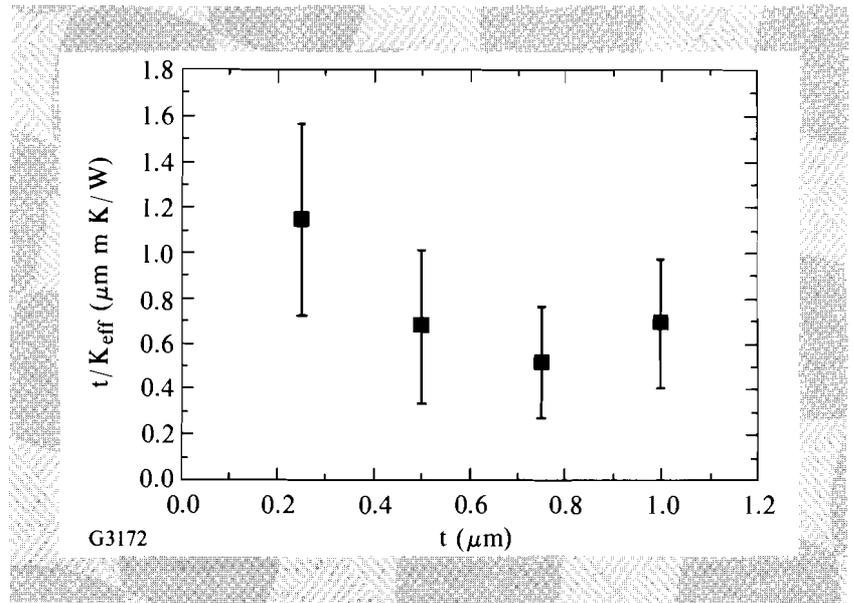

G3172

Fig. 49.19
Plot of Eq. (4) for e-beam-evaporated ZrO$_2$.
Compare with behavior shown in Fig. 49.15.

To find the source of this anomaly, the microstructure of the evaporated films was investigated. Figure 49.20 shows a TEM of a cross section of a ZrO_2 film. The film has a crack associated with the sample preparation, but more relevant is the fact that film is denser near the substrate (bottom of the micrograph) and becomes more obliquely columnar near the free surface. This situation would predict a higher thermal conductivity for the material nearer the substrate (the denser region), which is counter to the measurements of K_{eff}. Another possible source for the observed values of K_{eff} is the change in crystal structure with thickness often observed for ZrO_2 films.[17]

The three common polymorphs of ZrO_2 exhibit different thermal conductivities,[18] shown in Table 49.II. Most interesting is the value for cubic ZrO_2, a factor of two lower than the others. While transmission electron diffraction did not distinguish clearly the crystal structure of various regions of the films, IR spectroscopy shows the variation of crystal structure through the films. Figure 49.21 shows the transmission IR scans for each of four regions of a 1-μm-thick film taken for the frequency range 800–200 cm^{-1}. Each curve represents only 2500 Å of film material, and by comparing absorption peaks with previous data,[19] we can determine the crystal structure of each portion of the film. The 2500 Å curve shows a rather featureless region, indicating a large quantity of amorphous material, while the 5000 Å curve shows the emergence of some cubic material. The cubic material fades away and is replaced by monoclinic material for the two curves representing the regions of the films closest to the free surface.
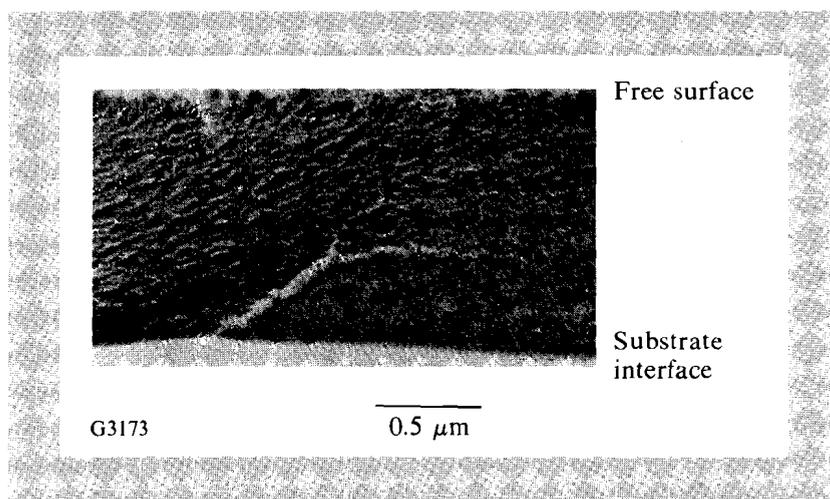

Fig. 49.20
TEM of ZrO_2 film cross section.

We conclude that the films are becoming less cubic and more monoclinic as deposition proceeds, and that an amorphous phase is present, especially near the substrate surface. Since amorphous materials typically show thermal conductivities suppressed by an order of magnitude from their crystalline counterparts;[20] the thinner films, consisting of cubic and amorphous material, are naturally poorer conductors of heat than the thicker films, containing the monoclinic phase.

Annealing is often used to crystallize and stabilize ZrO_2 films, with the added attraction that the thermal conductivity should also increase. Future work will include annealing of the ZrO_2 films to determine the effect on thermal conductivity and microstructure.

Table 49.II: Thermal conductivity of ZrO_2 polymorphs.[18]

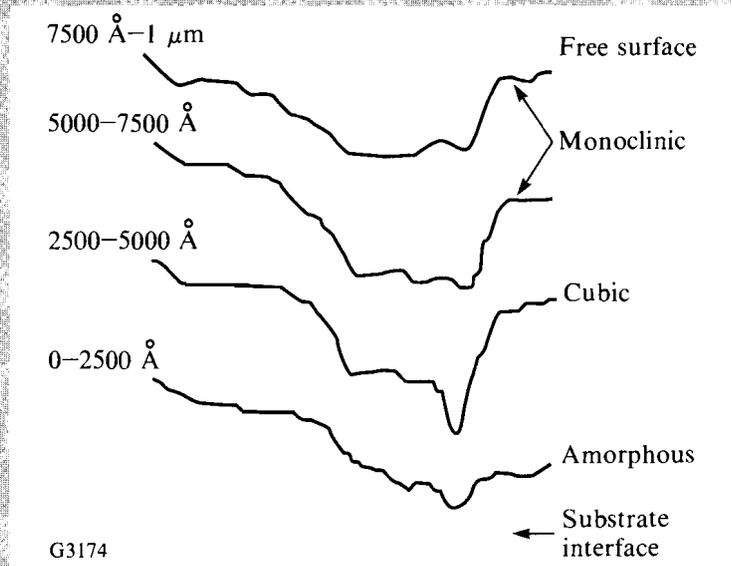| Crystal Structure	Thermal Conductivity (W/mK)
cubic	1.8
tetragonal	4.8
monoclinic	5.2

G3225

Fig. 49.21
Transmission IR scans for portions of evaporated ZrO_2 film. Each segment is 2500 Å, with the bottom curve corresponding to the film segment closest to the substrate.

$YBa_2Cu_3O_{7-\delta}$—Intrinsic Anisotropy and Hillock Growth

$YBa_2Cu_3O_{7-\delta}$, a ceramic, high-temperature superconductor, has been extensively studied in single-crystal platelet form. Most device applications now under development, including fast switches[21] and integrated circuits,[22] require that the material be in thin-film form. Knowledge of the thin-film thermal conductivity is important in predicting device stability.[23]

Thermal-conductivity measurements on $YBa_2Cu_3O_{7-\delta}$ single crystals have shown that thermal conductivity is anisotropic, and arises from different carrier combinations depending on crystal orientation.[24]

In the a-b, or superconducting planes, the thermal conductivity at room temperature typically varies from 8–12 W/mK, with 45% of the heat transport supplied by phonons and the remainder by electrons. Along the c axis, the thermal conductivity ranges from 1–2 W/mK with 95% of the heat carried by phonons. Another important effect is the oxygen content, or value of δ, which is directly related to the superconducting transition temperature.[25]

31

This factor accounts for some of the variation within a given direction, mentioned previously. Other defects do not affect the thermal conductivity of this material significantly at room temperature,[26] since the phonon mean free path is sufficiently small that defects such as stacking faults, twins, or grain boundaries would have to be much more closely spaced than is commonly observed in order to have a significant effect.

The films studied here were sputtered[27] from a ceramic source onto single-crystal (100) MgO substrates held at 730°C. XRD indicated that the films were oriented with the c axis perpendicular to the plane of the films. The thermal-comparator method yielded a thermal-conductivity value of 0.26 W/mK, which because of the film orientation must be a c-axis value. The Wiedemann-Franz-Lorenz conversion resulted in in-plane, or a-b plane values enumerated in Table 49.III.

Table 49.III: Thermal conductivity and superconducting transition temperatures for $YBa_2Cu_3O_{7-\delta}$ films.

Thickness (Å)	$K_\perp$, W/mK (comparator)	$K_\parallel$, W/mK (W-F-L)	T_c, K
2500		4.4	77
5000		4.5	83
7500	0.26	2.4	87
10,000		2.9	84

G3226

In both directions, the thermal conductivity is significantly depressed from the single-crystal values, but the anisotropy present in the single-crystal material is preserved in the thin films, with a slightly greater reduction observed perpendicular to the plane of the films. The values of the superconducting transition temperatures indicate that the films are close to stoichiometric, in fact that δ is around 0.2. Therefore, lack of stoichiometry is not a primary source of thermal resistance in the films.

The SEM cross section in Fig. 49.22 reveals a more likely reason for the lower thermal-conductivity values of the films. The very distinct hillocks on the film surface were analyzed by energy-dispersive spectroscopy, and showed higher barium and copper content than occurred in the film proper. The yttrium content is about the same, and the relative oxygen content could not be analyzed. The hillock material is, therefore, a distinct phase from the rest of the film, likely rich in $BaCuO_2$ and possibly CuO_2, and hence a probable source for lowered thermal conductivity.

Many other materials show anisotropic thermal-conductivity behavior in single-crystal form, which would be expected to exist in oriented thin-film form as well. Some examples include[28-29] rutile TiO_2 (K_a = 5.5 W/mK,
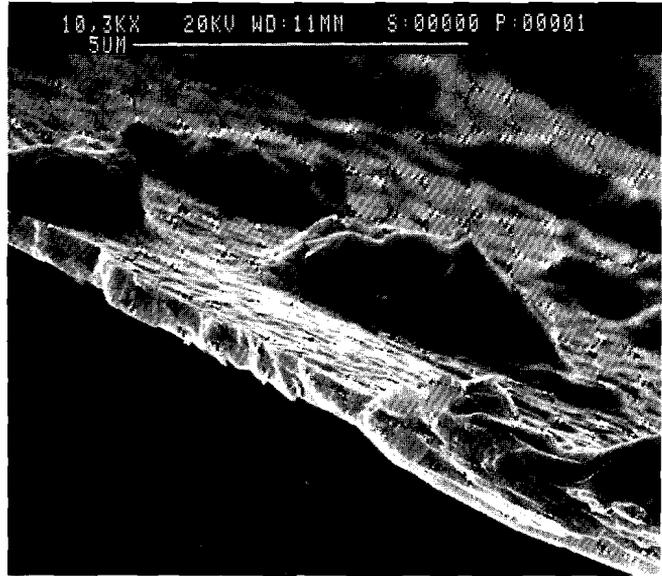
Fig. 49.22
SEM of $YBa_2Cu_3O_{7-\delta}$ cross section showing
hillocks on film surface.

G3175

$K_c = 7.6$ W/mK), quartz SiO_2 ($K_a = 4.5$ W/mK, $K_c = 8.7$ W/mK), and graphite ($K_a = 355$ W/mK, $K_c = 89$ W/mK). Also, the phase separation, which resulted in hillock formation in this case, is often observed during thin-film deposition of superconducting ceramics of other compositions.[30]

AlN—The Effect of Phonon Mean-Free-Path-Scale Scattering

AlN in single-crystal form exhibits a very high room-temperature thermal conductivity[31] of 320 W/mK. Since the phonons, the primary heat carriers in AlN, have a very long mean free path, study of this material provides a good opportunity for illustration of phonon-scattering events as sources of thermal resistance.

AlN was sputtered from a ceramic target onto glass substrates. When measured perpendicular to the plane of the film using the thermal comparator, the thermal conductivity of the film was 16 W/mK.[32] This decrease of more than an order of magnitude from the bulk value is drastic, but has been confirmed in previous measurements for AlN films.[33,34]

One common source of thermal resistance in AlN is the presence of vacancies that must form to conserve charge upon the introduction of oxygen impurities. A very small addition of oxygen is theoretically predicted to cause a large drop in the thermal conductivity. This effect can be calculated using the following expression for time between phonon scattering events $\tau(x)$:

$$\tau^{-1}(x) = \frac{x^4 k_B^4 T^4}{4\hbar^4 \pi v^3} f(1-f) \left[\left(\frac{\Delta M}{M} \right)^2 + \epsilon \left(\frac{\Delta \delta}{\delta} \right)^2 \right], \tag{6}$$

where variables are defined as for Eq. (2), with $\Delta M/M$ the fractional change in mass caused by the impurity introduction, $\Delta\delta/\delta$ the strain change, ϵ an empirical constant, and f the impurity atom fraction. Note that for vacancies, the term

$\Delta M/M$ is large, and substitution of Eq. (6) into Eq. (2) predicts a large drop in thermal conductivity, which is shown graphically in Fig. 49.23. XPS showed that the films studied here contain about 1-at.-% oxygen impurity, which accounts for a decrease in thermal conductivity of 50%. This is, therefore, a significant source of phonon scatter and thermal-conductivity reduction.

We must also consider the interruption of phonons by interaction with internal boundaries, such as grain boundaries, and external boundaries, such as the film surfaces. In this case, τ may be expressed

$$\tau^{-1} = v/d \, . \tag{7}$$

If this expression is substituted into Eq. (2), we obtain the dependence of thermal conductivity on grain size or film thickness for AlN, shown in Fig. 49.24.

Figure 49.25 shows a plan view of a typical AlN film. Note that the very small grain size of 30 nm may be expected to significantly contribute to thermal resistance through grain boundary scattering. However, the TEM cross-sectional micrograph shown in Fig. 49.26 shows that the grains extend through the thickness of the film. Since the comparator measures thermal conductivity in that direction, it is unlikely that the mean free paths of the phonons in question are interrupted by "bouncing" off grain boundaries as they travel perpendicular to the film plane.

More likely to cause phonon scatter are the upper and lower surfaces of the film. In fact, at room temperature, theory predicts a reduction in thermal conductivity for boundary scattering shown in Fig. 49.24. For boundaries separated by 1 µm, thermal conductivity is reduced at room temperature by 20%, and an even greater reduction occurs for thinner films.

Another important feature of the thin film cross section of Fig. 49.26 is that near the substrate, there is an apparently disordered region. Assuming that this disorder is an amorphous, near-substrate region often associated with thin-film deposition, a rather pronounced effect would be expected on $K_\perp$. This is because perpendicular to the film plane

$$\frac{t}{K_\perp} = \frac{t_a}{K_a} + \frac{t_c}{K_c} \, , \tag{8}$$

where t is the film thickness, t_a is the thickness of the disordered region, t_c is the thickness of the crystalline region, K_a is the thermal conductivity of the amorphous material, and K_c is the thermal conductivity of the crystalline region. If we assume that the thermal conductivity of the amorphous region is about an order of magnitude lower than that of the crystalline region,[20] and from Fig. 49.25 that the amorphous region takes up about 20% of the total thickness, then Eq. (8) predicts that the introduction of the disordered region near the substrate reduces $K_\perp$ an additional 64%.

Finally, with all nanocrystalline materials, we must consider the amorphous nature and the volume fraction of material occupied by grain boundaries. The

Fig. 49.23
Theoretical dependence of AlN thermal conductivity on oxygen content, calculated from Eqs. (6) and (2).
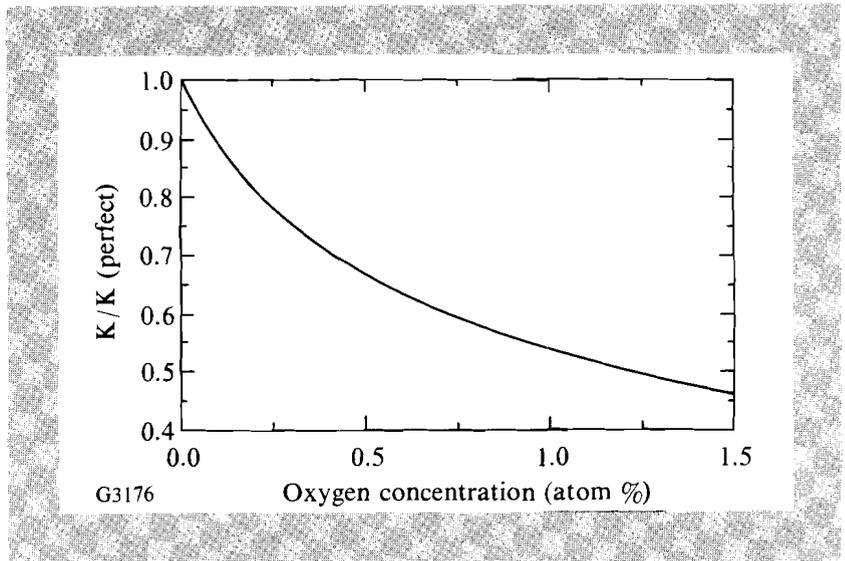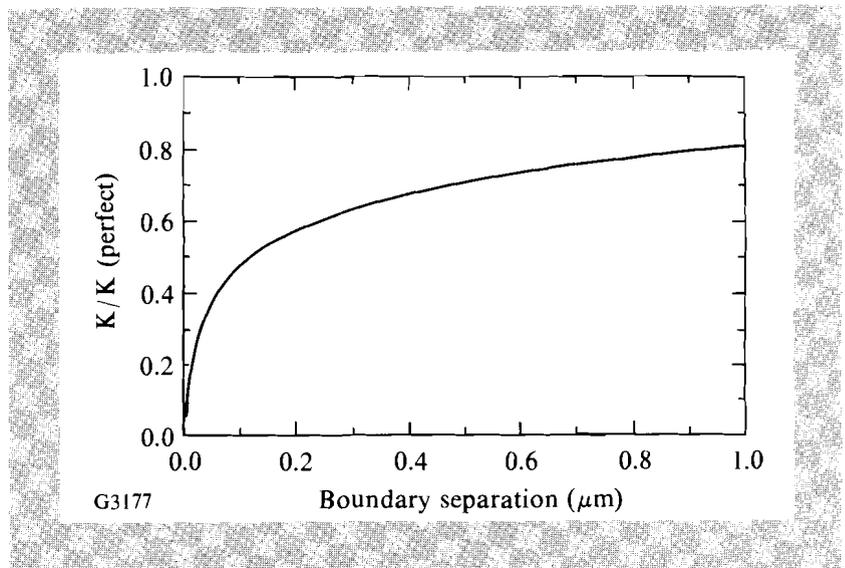
Fig. 49.24
Theoretical dependence of AlN thermal conductivity on interface separation (e.g., grain size or film thickness), calculated from Eqs. (7) and (2).

grain boundaries in Fig. 49.25 appear white because no diffraction of the electron beam has occurred, i.e., they are amorphous. This is consistent with models[35] for nanocrystalline microstructures, and of interest is the volume fraction of material that these amorphous regions occupy. Since amorphous materials have much lower thermal conductivity than crystalline materials (because of the reduction of the phonon mean free path to approximately the interatomic spacing), any material containing a significant volume fraction of amorphous regions should show a drop in thermal conductivity. Perpendicular to the plane of the film, these amorphous regions would have parallel heat paths and would lower the conductivity as resistors in parallel:

$$K_{\perp} = V_a K_a + V_c K_c \ , \tag{9}$$

where V_a and V_c are the volume fractions occupied by the amorphous (grain boundary) regions and the crystalline regions, respectively. In a material with a
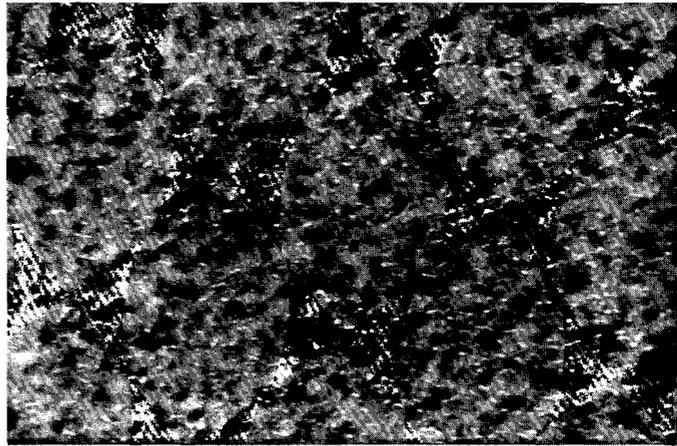
35

Fig. 49.25
Plan view TEM of sputtered AlN film.

G3178   0.1 μm

Fig. 49.26
TEM of sputtered AlN, showing a cross section
of the film.

G3179   1 μm

grain size of 1–10 nm, the amorphous grain boundaries occupy 50% of the volume.[35] If we conservatively estimate that for the AlN films the grain boundaries occupy 10% of the volume, Eq. (9) predicts a decrease in thermal conductivity of about 9%.

If we consider all of the thermal-resistance sources identified for AlN, we can account for an expected thermal conductivity of about 50 W/mK, still higher than the observed value. One likely source of the lower measured value is a probable overestimate for K_a, the thermal conductivity of amorphous AlN. Because no data based on actual measurements is available, we have estimated an order-of-magnitude reduction from the crystalline form based on SiO_2 data.[20] However, for a material with a high Debye temperature such as AlN ($\Theta_D = 950$ K), at room temperature, the difference between the amorphous and crystalline values of thermal conductivity is likely to be more than an order of magnitude.[36] Some additional unaccounted for thermal-resistance sources may also be responsible, such as undetected impurities.

So, for AlN, we have identified several contributions to thermal resistance, including impurities, a dimensional (thickness) effect, the disordered interfacial region, and the nanocrystalline microstructure. Except for the thickness effect, these factors may be controlled during deposition of the films.

Other film systems for which the mechanisms discussed for AlN are expected to be important include those with long phonon and/or electron mean free paths, such as crystalline metals and covalent ceramics including SiC, Al_2O_3, and diamond.

Summary

Experimental results and suggestions for increasing thermal conductivity for each of the systems studied here are shown in Table 49.IV. In general, we have found that

(1) Primary mechanisms of thermal resistance in thin films vary depending upon film material and deposition conditions.

    (a) Columnar microstructure introduces a strong thermal-conductivity anisotropy caused by the introduction of intercolumnar contacts.

    (b) Changes in crystal structure during thin-film deposition can introduce uncertainty in extracting thermal-conductivity values.

    (c) Intrinsic thermal-conductivity anisotropy carries over to thin-film form if the films are highly oriented.

    (d) Hillock growth of a second phase reduces thermal conductivity.

    (e) For materials with long heat-carrier mean free paths, (usually characterized by high Debye temperatures and high intrinsic thermal conductivities), many microstructural defects contribute strongly to thermal resistance, particularly point defects and 2-D boundaries.

    (f) Because they possess a heat-carrier mean free path on the order of the interatomic distance, amorphous materials or materials with amorphous regions always exhibit thermal-conductivity values significantly lower than their crystalline counterparts.

(2) Thermal conductivity of thin films can be optimized by identifying important system parameters and adjusting film-deposition conditions. The resulting improved conductivity should aid the goal of improving laser-damage resistance.

Table 49.IV: Summary of results.

Film Material	K_{film} (W/mK)	Thermal-Resistance Mechanisms	Suggested Remedy
RE-TM	4.3–7.3 $(K_\perp)$ 0.3–5.0 $(K_\parallel)$	intercolumnar contacts	increase deposition temperature, decrease deposition pressure
ZrO_2	? (anomalous)	crystal-structure variations	anneal to obtain monoclinic or tetragonal phase
$YBa_2Cu_3O_{7-\delta}$	0.26 $(K_\perp)$ 2.4–4.5 $(K_\parallel)$	intrinsic anisotropy, hillock growth	reduce hillocks by encouraging equilibrium growth
AlN	16	impurities, thickness effect, disorder at interface, amorphous grain boundaries	improve vacuum cleanliness, heat substrate, increase grain size

G3227

REFERENCES

1. A. H. Guenther and J. K. McIver, Thin Solid Films **163**, 203 (1988).

2. J. C. Lambropoulos, M. R. Jolly, C. A. Amsden, S. E. Gilman, M. J. Sinicropi, D. Diakomihalis, and S. D. Jacobs, J. Appl. Phys. **66**, 4230 (1989).

3. D. L. Decker, L. G. Koshigoe, and E. J. Ashley, in *Laser Induced Damage in Optical Materials: 1984, Natl. Bur. Stand. (U.S.), Spec. Publ. 727* (Government Printing Office, Washington, DC, 1986), pp. 291-297.

4. P. G. Klemens, in *Solid State Physics*, edited by F. Seitz and D. Turnbull, *Advances in Research and Applications*, Vol. 7 (Academic Press, New York, 1958), pp. 1–98.

5. W. D. Kingery, H. K. Bowen, and D. R. Uhlmann, in *Introduction to Ceramics*, 2nd ed. (Wiley, New York, 1976), pp. 634–643.

6. J. Callaway, Phys. Rev. **113**, 1046 (1959).

7. P. G. Klemens, Proc. Phys. Soc. LXVIII **12-A**, 1113 (1955).

8. P. G. Klemens, Can. J. Phys. **35**, 441 (1957).

9. R. B. Dinwiddie and D. G. Onn, in *Advanced Electronic Packaging of Materials*, edited by A. F. Barfknecht, J. P. Partridge, C. J. Chen, and C.-Y. Li (Materials Research Society, Pittsburgh, PA, 1990), Vol. 167, pp. 241–246.

10. R. K. Williams *et al.*, J. Appl. Phys. **62**, 2778 (1987).

11. R. J. Anderson, J. Appl. Phys. **67**, 6914 (1990).

12. J. A. Thornton, in *Modeling of Optical Thin Films* (SPIE, Bellingham, WA, 1987), Vol. 821, pp. 95–103.

13. L. J. Shaw-Klein, T. K. Hatwar, S. J. Burns, S. D. Jacobs, and J. C. Lambropoulos, J. Mater. Res. **7** (to be published).

14. R. W. Heimburg and K. N. Tong, in *Thermal Conductivity, Proceedings of the Eighth Conference*, edited by C. Y. Ho and R. E. Taylor (Plenum Press, New York, 1969), pp. 527–540.

15. A. G. Dirks and H. J. Leamy, Thin Solid Films **47**, 219 (1977).

16. D. T. Morelli, C. P. Beetz, and T. A. Perry, J. Appl. Phys. **64**, 3063 (1988).

17. E. N. Farabaugh *et al.*, J. Vac. Sci. Technol. A **5**, 1671 (1987).

18. D. P. H. Hasselman *et al.*, Am. Ceram. Soc. Bull. **66**, 799 (1987).

19. C. M. Phillippi and K. S. Mazdiyasni, J. Am. Ceram. Soc. **54**, 254 (1971).

20. W. D. Kingery, H. K. Bowen, and D. R. Uhlmann, in *Introduction to Ceramics, 2nd ed.* (Wiley, New York, 1976), p. 625.

21. W. R. Donaldson, A. M. Kadin, P. H. Ballentine, and R. Sobolewski, Appl. Phys. Lett. **54**, 2470 (1989).

22. R. Simon, Phys. Today, June 1991, 64.

23. M. I. Flik and C. L. Tien, *Annual Review of Heat Transfer*, edited by C. L. Tien (Hemisphere Publishing Corp., New York, 1990), Vol. 3, pp. 115–144.

24. S. T. Hagen, Z. Z. Wang, and N. P. Ong, Phys. Rev. B **40**, 9389 (1989).

25. R. J. Cava *et al.*, Physica C **165**, 419 (1990).

26. R. K. Williams *et al.*, J. Appl. Phys. **66**, 6181 (1989).

27. P. H. Ballentine *et al.*, J. Vac. Sci. Technol. A **9**, 1118 (1991).

28. *CRC Handbook of Chemistry and Physics, 51st ed.*, edited by R. C. Weast (The Chemical Rubber Company, Cleveland, OH, 1970), p. E-5.

29. J. F. Nye, *Physical Properties of Crystals* (Clarendon Press, Oxford, 1964) p. 196.

30. T. N. Blanton, C. L. Barnes, and M. Lelental, Physica C **173**, 152 (1991).

31. G. A. Slack *et al.*, J. Phys. Chem. Solids **48**, 641 (1987).

32. L. J. Shaw-Klein, S. J. Burns, and S. D. Jacobs, in *Electronic Packaging Materials Science V*, edited by E. D. Lillie, P. S. Ho, R. Jaccodine, and K. Jackson (Materials Research Society, Pittsburgh, PA, 1991), Vol. 203, pp. 235–240.

33. D. Raasch and S. Klahn, J. Magn. & Magn. Mater. **93**, 365 (1991).

34. R. P. Tye (private communication).